Minor structural modifications to alchemix influence mechanism of action and pharmacological activity

Qasem M. A. Abdallah[a], Roger M. Phillips[a], Fredrik Johansson[b,c], Thomas Helleday[c], Laura Cosentino[a], Hamdy Abdel-Rahman[a], Jasarat Etzad[a], Richard T. Wheelhouse[a], Konstantinos Kiakos[d], John P. Bingham[d], John A. Hartley[d], Laurence H. Patterson[a], Klaus Pors[a,]*.

[a]*Institute of Cancer Therapeutics, University of Bradford, West Yorkshire, BD7 1DP, U.K.*

[b]*Science for Life Laboratory, Division of Translational Medicine and Chemical Biology, Department of Medical Biochemistry and Biophysics, Karolinska Institute, Stockholm, Sweden.*

[c]*Department of Genetics, Microbiology and Toxicology, Stockholm University, S-106 91 Stockholm, Sweden.*

[d]*Cancer Research UK Drug-DNA Interactions Research Group, UCL Cancer Institute, London, WC1E 6BT, U.K.*

*Address for correspondence: Institute of Cancer Therapeutics, University of Bradford, Bradford, West Yorkshire, BD7 1DP, U.K., Phone: +44 (0)1274 236 482. Fax: +44 (0)1274 233 234. Email: k.pors1@bradford.ac.uk

Category: Antibiotics and Chemotherapeutics

Abstract

Alchemix is an exemplar of a class of anthraquinone with efficacy against multidrug resistant tumors. We have explored further the mechanism of action of alchemix and investigated the effect of extending its side arm bearing the alkylating functionality with regard to DNA binding and activity against multidrug resistant cancer cells. Increasing the distance between the intercalating chromophore and the alkylating functionality of ICT2901 (propyl), ICT2902 (butyl) and ICT2903 (pentyl), led to a higher number of DNA alkylation sites, more potent topoisomerase II inhibition and generated more apoptotic and necrotic cells when analysed in p53-proficient HCT116 cells. Intriguingly, alchemix, the compound with the shortest distance between its intercalative chromophore and alkylating functionality (ethyl), did not conform to this SAR. A different toxicity pattern against DNA repair defective CHO cell lines as well as arrest of cells in G1 supports a somewhat distinct mode of action by alchemix compared with its analogues. Importantly, both alchemix and ICT2901 demonstrated greater cytotoxic activity against anthraquinone-resistant MCF-7/adr cells than wild-type MCF-7 cells. Subtle synthetic modification in this anthraquinone series has led to significant changes to the stability of DNA-compound complexes and cellular activity. Given that the failure of chemotherapy in the clinic is often associated with MDR, the results of both alchemix and ICT2901 represent important advances towards improved therapies.

Keywords: anthraquinone, H2AX phosphorylation, MDR, topoisomerase II, NER, p53.

Abbreviations

CHO	Chinese Hamster Ovary
CT DNA	Calf thymus DNA
DMSO	Dimethyl sulphoxide
DSB	Double strand break
H2AX	Histone-2AX
MDR	Multidrug resistance
MTT	(3-(4,5-dimethylthiazol-2-yl)-2,5-diphenyltetrazolium bromide
TdT	Terminal deoxynucleotidyl transferase
Topo II	Topoisomerase II
TUNEL	Terminal deoxynucleotidyl transferase-mediated dUTP nick end labeling
SAR	Structure-activity relationship

1. **Introduction**

Topoisomerase II (topo II) inhibitors are often based on planar aromatic pharmacophores, which constitute an important class of clinically useful anti-tumor agent. Daunorubicin, doxorubicin, epirubicin and mitoxantrone are established drugs that are based on a tricyclic anthraquinone pharmacophore, which is a prerequisite for topo II poisoning [1]. Substantial work has defined the relationship between the basic aminoalkylamino sidechains and configuration of functional groups attached to the 1,4-disubstituted pharmacophore of mitoxantrone [1-7]. The clinical success of the anthraquinone-based anticancer drugs is tempered by their failure in tumors that express the ABCB1 (MDR1) gene [8-10], or exhibit downregulation/mutation [11] or phosphorylation [12] of topo II. In an attempt to overcome these resistance mechanisms, we have previously reported 1,4-disubstituted chloroethylaminoanthraquinones as a hybrid class of agents containing DNA intercalating and alkylating functionalities [13, 14], of which one agent, alchemix (Figure 1) possesses substantial anticancer activity against doxorubicin- (A2780AD) and cisplatin-resistant (A2780/cp70) tumor xenografts in mice [15]. In particular, symmetrical (two identical sidechains) 1,4-disubstituted anthraquinones with alkylating groups on both sidechains lose cytotoxic potency in multidrug-resistant (MDR) cancer cells, but non-symmetrical mixed sidechain-configured anthraquinones, typified by alchemix, remain effective against such malignant cells [14, 15].

Figure 1

This study expands the knowledge of the DNA binding properties of alchemix and its cellular pharmacology. To explore these phenomena, three novel analogues of alchemix were prepared (Figure 1), which would provide a platform for a better understanding of the optimum requirements for DNA adduct formation, topo IIα inhibition and cytotoxicity.

2. Materials and methods

2.1. Synthesis of target compounds

The synthesis of alchemix and the three novel anthraquinones was carried out using methodology previously reported [13]. Briefly, *ipso*-substitution of 1-(2-(dimethylamino)ethylamino)-4-fluoro-5,8-dihydroxyanthracene-9,10-dione with the respective bis(hydroxyl)-aminoalkylamine generated bis-substituted hydroxyethyl precursors, which were converted to the target chloro compounds using triphenylphosphine-carbon tetrachloride complex (PPh_3-CCl_4). Full experimental methodology and characterisation of ICT2901, ICT2902 and ICT2903 can be found in supporting information. All compounds were stored as hydrochloride salts at –20 °C under anhydrous conditions prior to use.

2.2. DNA binding studies

Doxorubicin, mechlorethamine (*N*-methyl-*N,N*-bis(2-chloroethyl)amine), 3-(4,5-simethyl- 2-thiazolyl)-2,5-diphenyl-*2H*-tetrazolium bromide (MTT), ammonium persulphate (APS), and sequagel 6 (concentrate) were obtained from Sigma-Aldrich Chemicals (Gillingham, U.K.). Plasmid DNA pBR322 (0.25 U/μL) was purchased from New England Biolabs (Herts, U.K.), γ^{32}P-ATP (500 Ci/mmol), 5´-TATGCGACTCCTGCATTAGG-3´ primer (10 pm/μl), dNTP mix (2.5 mM), T4 polynucleotide kinase (5 U/μl), bacterial alkaline phosphatase (BAP) (150 U/μl), *Taq* DNA polymerase (5 U/μl) and Hind III (15 U/μl), BamH1 and SalI restriction

enzymes were purchased from Promega, (Southampton, UK). BIO-RAD spin columns were obtained from BIO-RAD Laboratories, (Beckenham, UK).

2.2.1. Taq polymerase stop assay

This experiment has previously been described [13, 16]. Briefly, the following constituents were added to a PCR tube: 0.2 % gelatine (5 µl), 25 mM $MgCl_2$ (10 µl), 10 × Taq polymerase buffer buffer (10 µl), 2.5 mM dNTP mix (10 µl), dH_2O (8 µl) and 0.5µg drug-treated (1-100 nM) linearised pBR322 DNA (50 µl). The latter was generated after incubation for 1 h at 37 °C. To the mixture (93 µl) was then added a synthetic 20 base oligonucleotide primer that binds to the sequence 621-640 of the 273 base pair BamH I/Sal I fragment of pBR322 (bases 375-650), *Taq* polymerase (2 µL, 5 U/µl), and the final mixture was vortexed. The thermocycler was programmed to: (1) 95 °C for 5 min, (2) 95 °C for 1 min, (3) 58 °C for 1 min, (4) 74 °C for 1 min and an additional 1 min per cycle. Step 2–4 were repeated 29 times before denaturing at 94 °C for 5 min followed by 10 min at 25 °C. The samples were then transferred into sterile eppendorf vials and the DNA precipitated with 3 volumes of ethanol (95 %, 300 µl) and NaOAc (3 M, 2 µl), vortexed and cooled in dry ice bath for 10 min before being centrifuged at 13,000 rpm for 10 min. The supernatant was removed and the samples were washed with ethanol (70 %, 150 µl), vortexed, centrifuged at 13,000 rpm for 10 min and the supernatant removed. The wash was repeated and the samples lyophilized. Each dried sample was re-suspended in formamide dye (4 µl), heated to 95 °C for 3 min and cooled in an ice-bath to denature the DNA. The samples were loaded into the wells of a 6% denaturing polyacrylamide gel and electrophoresis was performed in TBE buffer at 1600-2000 V (approx. 2–3 h, 55 °C) using vertical glass electrophoresis plates. The resulting gel was then transferred onto a Whatman 3MM filter paper and one layer of DE81, covered in film wrap

and dried on a BIO-RAD 583 gel drier for approximately two h. Once dry, the gel was exposed to a Kodak Hyperfilm for 24 h before development.

2.2.2. UV thermal melting studies of ligands and calf thymus DNA

The protocol used to determine thermal denaturation profiles for double-stranded calf thymus (CT) DNA and ligand-induced melting temperature shifts (ΔT_m) has been previously described [17, 18]. CT DNA (sodium salt) was purchased from Sigma and used without further purification; the buffer used was aqueous sodium phosphate (Na_2HPO_4/NaH_2PO_4 10 mM, Na_2EDTA 1 mM, pH 7.00), CT DNA solutions were quantitated spectrophotometrically using ε_{260} = 12 824 M(base pairs)$^{-1}$ cm^{-1} at 260 nm. Anthraquinones were dissolved in DMSO and stock solutions stored at 4 °C. Ligand-DNA mixtures were prepared by carefully adding ligand stock solution to DNA to achieve a final concentration of 50 μM (bp) DNA and 10 μM anthraquinone, ensuring that the final concentration of DMSO was < 1% v/v. DMSO calibration curves were used to correct the T_m values.

UV DNA melting curves were determined using a Varian-Cary 400 Bio UV/vis spectrophotometer equipped with a Peltier temperature controller. Heating was applied at a rate of 1 °C/min in the range 40–95 °C, the absorbance was monitored continuously at 260 nm. All melts were performed in 1 cm path length, masked quartz cells. For kinetic experiments, working solutions of DNA-anthraquinone mixtures at the fixed 5:1 molar ratio were incubated at 37 °C and evaluated at set time points of 0, 4, 8 and 24 h. Results for each compound are means of three separate determinations.

2.3. Topoisomerase II decatenation assay

Decatenation of kinetoplast DNA (kDNA; from Crithidia Fasciculata and purchased from TopoGEN) was used to assay the level of topo IIα inhibition. The standard topo IIα

(purchased from affymetrix/USB) reaction mixture contained 10 mM Tris-HCl, pH 7.9, 175 mM KCl, 5 mM MgCl2, 0.1 mM EDTA, 0.2 mM dithiothreitol, 2.5% glycerol, 1 mM ATP, 30 µg/ml BSA, 0.1 µg kDNA and sterile distilled water to 20 µl. The reaction was incubated with 4U of topo IIα at 37 °C for 30 min and terminated by the addition of 5 µl of stop buffer (10% w/v sodium dodecyl sulphate, 50% glycerol, 0.025% bromophenol blue). The reaction mixture was centrifuged at 14000 g for 10 sec. The blue mixture was loaded directly onto 1% horizontal agarose gel and electrophoresed in 90 mM Tris-base, pH 8.3, 2.5 mM EDTA. Gels were electrophoresed for 4 h at 6 V/cm and photographed under UV transillumination for 30 sec.

2.4. Chemosensitivity

All drugs were dissolved in DMSO to obtain stock solutions at 10 mM, aliquoted and stored at –20 ^{o}C prior to use. MCF-7, MCF-7/adr, HCT116$^{p53+/+}$ and HCT116$^{p53-/-}$ cancer cell lines (obtained from ATCC) were routinely maintained as mono-layered cultures in RPMI 1640 medium supplemented with 10 % fetal bovine serum, 2 mM L-glutamine and 1 mM sodium pyruvate. The arrest of cell growth was determined by the MTT assay as previously reported [19]. Briefly, cells were plated in 96-well plates with 200 µl of cell suspension (0.5×10^4 cell/ml) per well. Cells were left to adhere overnight at 37 $^{\circ}$C in a humidified incubator (5% CO_2 and 95% air) and then exposed to a suitable range of drug concentrations for 1 h or 96 h in complete RPMI 1640 medium. Following drug exposure, cells were washed three times with Hanks Balanced Salt Solution and complete growth medium (200 µl/well) was added. Chemosensitivity was determined using the MTT assay 4 days later. For both 1 h and continuous drug exposures, MTT (20 µl, 5mg/ml) was added to each well and the plates incubated at 37 $^{\circ}$C for 4 h. All medium was removed and formazan crystals were dissolved in 150 µl of DMSO. The absorbance of the resulting solution was measured at 540 nm using a

multiwell spectrophotometer (Multiskan EX; Thermo Fisher Scientific, Waltham, MA, USA). Survival and chemosensitivity were expressed as IC_{50} values. All experiments were repeated in triplicate.

2.5. γH2AX and cell cycle analysis

$HCT116^{p53+/+}$ colorectal carcinoma cells were exposed to drug concentrations equal to the IC_{80} value for a 1 h drug exposure followed by removal of the drug and recovery in fresh medium for 3, 24 or 48 h. Cells were collected by trypsinization and fixed in ice-cold methanol at –20 °C for 30 min. Cells were collected by centrifugation and washed in PBS. Following inhibition of non-specific antibody binding by incubation in staining buffer (5% BSA in PBS) for 10 min at room temperature, cells were incubated for 60 min at room temperature with anti-phospho-histone H2AX antibody, Ser 139, (Cell Signaling Technology, USA; diluted 1:50 in staining buffer). Cells were washed in staining buffer and immunoreactivity was detected using an anti-rabbit Alexa Fluor®-488 labeled secondary antibody (Cell Signaling Technology, USA; diluted 1:1000). Cells were further washed in staining buffer and resuspended in PBS containing propidium iodide (200 µg/ml; Sigma, Gillingham, UK) and RNase A (200 µg/ml; Invitrogen, Paisley, UK) at 37 °C for 30 min. Vials were placed on ice before analysis. Flow cytometry analyses were performed using a FACS-Calibur flow cytometer (BD Biosciences; San Jose, CA, USA). Data obtained from 10,000 cellular events were analyzed using the CellQuest software (BD Biosciences; San Jose, CA, USA).

2.6. Induction of cellular apoptosis and necrosis

$HCT116^{p53+/+}$ colorectal carcinoma cells were exposed to drug concentrations equal to the IC_{80} value for 1 h, followed by removal of the drug and recovery in fresh medium for 24 h.

Cells were collected by trypsinization and resuspended in PBS. Cell suspensions (100 µl) were applied to poly-L-lysine coated microscope slides and air-dried in a fume hood at room temperature. Slides were incubated in buffered formalin for 5 min at room temperature to fix cells and then washed twice with PBS. Apoptotic cells were detected using the DeadEnd Colorimetric TUNEL assay (Promega, USA) according to the manufacturer's instructions. At least 500 cells were counted per slide from 10 random areas and the resultant percentage of apoptotic cells determined.

For determination of necrosis, cell suspensions were mixed with equal volumes of Trypan Blue solution (0.4%, Sigma). The percentage of necrotic cells was then calculated by counting the proportion of blue versus unstained cells using a haemocytometer. All results are the mean of three independent experiments.

2.7. Studies in Chinese Hamster Ovary (CHO) cell lines

1 x10^4 CHO cells were seeded in a 96-well plate in 200 µl DMEM. After 24 h the cells were treated with indicated compounds for 120h. After treatments, the wells were rinsed twice with $HBSS^{++}$ (200 µl/well) before fixation for 20 min in 4% formaldehyde/1% $CaCl_2$, twice rinsing with distilled water before staining with 0.01% neutral red (NR) in water for 1 h. The plates were rinsed an additional three times in water followed by addition of 200 µl 1% acetic acid/50% ethanol added to each well for incubation for 30 min. Finally, absorbance was measured at 540 nm and data analysed as previously described [20].

3. Results

3.1. DNA sequence-selective alkylation and inter-strand cross-linking experiments

Compounds ICT2901, ICT2902 and ICT2903 were compared with alchemix for their ability to covalently adduct double-stranded DNA using the *Taq* polymerase stop assay [16]. Inhibition of DNA elongation, consistent with DNA alkylation, was detected down to 5 nM for ICT2902 and ICT2903 compared with 1 μM for mechlorethamine (Figure 2). The four alkylating anthraquinones demonstrated a strong preference for guanines, specifically the guanines that were flanked by a 5'-cytosine and a 3'-guanine residue (e.g. 5'-C*G*G; positions 536, 586 and 596 in Figure 2) and to a lesser extent at the second guanine in the same sequence (5'-CG*G*; positions 537, 587 and 597). A potentially important alkylation site was also observed at position 529 in the sequence 5'-C*G*T, which was not an alkylation site shared by mechlorethamine. In contrast, mechlorethamine showed a pattern of sequence selective alkylation as observed previously, with a preference for reaction within runs of contiguous guanines [21]. For example, alkylation was observed at 5'-T*GGG*C, which was not a target site for any of the four anthraquinones, suggesting that the 5'-TG or 5'-GG residue is not an ideal site for DNA intercalation to occur. Alkylation was observed, however, with all compounds at the guanine-rich sequence 5'-CGGGGG (bases 536-540) with the anthraquinones preferring alkylation of Gs at the 5' terminus of the G-tract and mechlorethamine the middle Gs. There was no apparent difference in sequence selectivity between alchemix and the three novel compounds ICT2901, ICT2902, and ICT2903 although qualitative differences in reactivity were evident. For example, compounds ICT2902 and ICT2903 with butyl (n = 3) or pentyl (n = 4) linkers respectively, revealed more intense bands at several alkylation sites including at base positions 536-540. None of the four agents was shown to cause DNA interstrand crosslinking in concentration-dependent (0.1–100 nM) experiments using a gel-based electrophoretic assay (Figure S1, Supporting Information).

Figure 2

3.2. DNA thermal denaturation studies

Reactivity of the four anthraquinones towards double-stranded DNA was assessed by measuring their capacity to modify the melting behavior (T_m) of calf thymus DNA. Using a 5:1 (50 μM DNA:10 μM compound) ratio and analysis of the "instant" (t = 0) DNA binding, the compounds were found to shift the DNA melting curve moderately (ΔT_m = 6.5-14.8˚C) (Table 1). Interestingly, notable differences in their DNA binding mode became apparent when studying time-dependent incubations at 37 °C for up to 24 h. Alchemix (n = 1) and ICT2901 (n = 2) exhibited the most stable interactions with DNA; the ΔT_m observed at t = 0 (11.0 and 14.8 °C, respectively) decreased only slightly after 24 h. In contrast, ICT2902 (n = 3) and ICT2903 (n = 4), compounds with the longer carbon sidechains, were less effective in stabilizing the DNA duplex at the onset of the experiment ($\Delta T_m \leq 7$ °C) but over the course of 24 h incubation, ΔT_m decreased in a near-linear fashion to zero (supporting information, Figure S2).

Table 1

3.3. Inhibition of topo IIα activity

The ability of the four compounds to inhibit topo IIα was measured using catenated kinetoplast DNA. The experiments was carried out as previously described using the anthraquinone-based clinical prodrug AQ4N and its metabolite AQ4 (topo IIα inhibitor) as negative and positive controls respectively [22]. All compounds were shown to completely inhibit topo IIα at 2.5 μM but at lower concentrations a dose-response was observed. Figure 3 shows that both ICT2902 and ICT2903 prevent the catenated kinetoplast DNA in migrating at 100 nM indicative of topo II inhibition. In contrast, alchemix is not able to inhibit the

formation of individual DNA circles and intermediate-sized catenated complexes whereas ICT2901 partly prevents decatenation.

Figure 3

3.4. Chemosensitivity

The response of cell lines to alchemix and its analogues are presented in Tables 2 and 3. Following a 1 h exposure, all four compounds showed comparative activity against p53 proficient and deficient HCT116 cell lines with resistance factors (RF, the ratio of IC_{50} values in $p53^{-/-}$ cells to $p53^{+/+}$ cells) ranging from 1.13 to 1.65 (Table 2). Similar results were obtained following a 96 h drug exposure although RF values increased modestly (1.59 to 3.26, Table 2). Of the four compounds evaluated, ICT2901 was the most potent following both a 1 and 96 h exposure against all cell lines evaluated (Tables 2 and 3). Potency generally decreased as the length of the side chain increased with the exception of alchemix where IC_{50} values typically fell within the range of IC_{50} values observed. Against the MCF-7 and MCF-7/adr cells, alchemix and ICT2901 were preferentially active against MCF-7/adr cells (Table 3). This contrast sharply with doxorubicin, which was significantly (> 45 fold) less active against MCF-7/adr cells (Table 3). ICT2902 was equitoxic against both cell lines whereas ICT2903 was less active against MCF-7/adr cells. Comparing the activity of all anthraquinones against cells following a 1 h and 96 h exposure, it is clear that differences in IC_{50} values are small in all cases. This is in marked contrast to doxorubicin where the IC_{50} values against MCF-7 cells are 218 ± 91 and 6.1 ± 2 μM for 96 and 1 h exposures respectively (Table 3).

Table 2

Table 3

3.5. Cell Cycle

The effect on cell cycle progression was investigated by flow cytometry in the HCT116$^{p53+/+}$ cell line exposed to IC_{80} drug concentrations for 1 h. Analysis of cell cycle progression was subsequently performed at time points 0, 3, 24 and 48 h after recovery in drug-free medium. No noticeable difference was observed immediately after drug exposure (t = 0 h) between the anthraquinone-treated cells and the non-treated controls (results not shown). However, a significant effect was observed after 24 and 48 h recovery time, with cells primarily arrested in G2 (Figure 4). Alchemix appeared to induce a significant accumulation of cells in G1 phase (51.8% *versus* 35.5% of control cells) after 3 h recovery, which was not evident with the other anthraquinones.

Figure 4

3.6. Cell death pathways

The induction of apoptosis and necrosis following the exposure of HCT116$^{p53+/+}$ cells to alchemix and the three derivatives is presented in Figures 5 and 6. Cells were exposed to compounds at IC_{80} for 1 h and after washing cells were incubated in drug-free medium for 24 h before assessing the level of apoptotic and necrotic cells. A SAR between the length of the hydrocarbon linker and number of apoptotic and necrotic cells was observed for the three derivatives. ICT2903, the compound with the longest linker (pentyl) induced the highest level

of apoptotic (9.4 ± 1.6 %) and necrotic (9.3 ± 2.6) cells. Intriguingly, alchemix was found outside this SAR, exhibiting the highest level of apoptotic cells (10.1 ± 0.2 %) of all four compounds.

Figure 5

Figure 6

3.7. γH2AX phosphorylation

HCT116$^{p53+/+}$ cells were used to evaluate the ability of the anthraquinones to induce DSBs. The HCT116 cells were exposed to anthraquinone concentrations equal to IC_{80} for 1 h, followed by a recovery period in fresh medium for 3, 24 or 48 h. A time-dependent increase in γH2AX phosphorylation was observed for all compounds bar ICT2901, which demonstrated noticeable activation after only 3 h (Figure 7).

Figure 7

3.8. Repair of DNA adducts in CHO cell lines

To establish the roles of DNA repair mechanisms in repairing adducts generated by the anthraquinones, a panel of Chinese hamster ovary (CHO) cell lines, with specific defects in DNA excision repair was employed. The sensitivity of the CHO cells to the anthraquinones was assessed using the DRAG assay [20]. Table 4 shows the sensitivity of the wild-type (AA8) and the DNA-defective repair CHO cell lines mutants to the respective anthraquinones

after 120 h exposure to increasing concentrations of the agent. Increased sensitivity for the three compounds tested (alchemix, ICT2901 and ICT2903) was observed in the UV4 cell line, which harbors a defect in the ERCC1 gene known to affect nucleotide excision repair (NER) repair pathways. In addition, alchemix was slightly more cytotoxic to cells defective in ERCC2 (2.1 fold) and XRCC1 (1.2 fold), which may be indicative of failure to repair transcription-coupled nucleotide excision repair and base excision repair (BER) respectively.

Table 4

4. Discussion

Alchemix is the prototype of a class of anthraquinone derivatives with a dual mode of action that combines DNA intercalating and alkylating properties. Alchemix has previously been shown to exhibit significant growth delay against anthracycline- and cisplatin-resistant xenografts [15]. This activity is derived from DNA intercalation, mono-alkylation and inhibition of topo IIα without inter-strand DNA cross-linking [13, 15]. Furthermore, unlike a classical topo IIα inhibitor such as doxorubicin, alchemix is neither a substrate for P-gp [15, 23] nor significantly affected by the lower levels of topo IIα present in resistant A2780/adr cells [24]. This study examined the nature of DNA binding by alchemix and subsequent cellular pharmacology. To that effect three novel analogues were designed to aid the interpretation of not only the DNA binding data, but also provide insights into how DNA injury may be recognized and cause downstream activation of cell death pathways.

The results presented in this report suggest that subtle modification to the sidechain carrying the alkylating group of alchemix has a profound effect on DNA binding. The four anthraquinones were assessed for DNA binding by measuring their induced effects on the UV thermal melting profiles (ΔT_m) of duplex-form CT DNA. All compounds were found to shift the DNA melting curve moderately at t = 0, however notable differences in the stabilization of

the DNA duplex were evident when studied over longer incubation times (Table 1). Alchemix (ethyl) and ICT2901 (propyl) exhibited the greatest stabilizing effect on DNA and the most persistent adducts, showing only a slight decrease in ΔT_m over 24 h. In contrast, the compounds with longer sidechains, ICT2902 (butyl) and ICT2903 (pentyl), were less effective DNA stabilants and over the course of 24 h incubation, ΔT_m decreased to zero. Drugs derived from the nitrogen mustard family are known to generate purine-sugar glycosidic linkages that become labile and prone to depurination over long exposure times or elevated temperatures [25]. Accordingly, it is possible that the longer and more flexible alkylating sidechains of ICT2902 and ICT2903 are responsible for achieving a higher number of G(*N*7) mono-adducts that are prone to depurination. Indeed, ICT2902 and ICT2903 were the most potent agents in the *Taq* polymerase footprinting assay, showing detectable DNA alkylation at 5 nM but still without the capacity to inter-strand cross-link DNA. ICT2903, alkylated all the guanines in the guanine-rich sequence 5'-GGGGG (bp = 536-540) and showed a modest preference for the 5'-peripheral guanines. In contrast, the nitrogen mustard, at ~200-fold higher dose, showed a preference for alkylating the central guanines in this sequence of contiguous guanines. This selectivity is due to enhanced nucleophilicity of the G(*N*7) nucleophiles in this sequence and is shared by many low molecular weight electrophilic drugs [21]. As such, it is apparent that the alkylation sites of mechlorethamine were modulated by tethering the bis-chloroethylamino moiety to the anthraquinone pharmacophore, indicating that the latter directed the site of covalent bonding. The higher potency of G alkylation by the butyl and pentyl linker compounds, suggests an improved compliance with the stereoelectronic requirements of the alkylation reaction. Despite of the higher potency in alkylating DNA, no correlation to cellular potency was apparent. Taken together, the results suggest that alchemix and ICT2901 with the shorter sidechains are able to bind to DNA in such a way that a stable DNA-drug non-covalent complex is obtained.

The anthraquinones showed dose-dependent anti-proliferative activity with IC_{50}<100 nM (Tables 2 and 3) against both sensitive and resistant HCT116 and MCF-7 human cancer cells. Generally, the anthraquinones were equitoxic after both short-term (1 h) and long-term (96 h) exposure. In contrast, doxorubicin was less active at 1 h than after 96 h in the MCF-7 cell line (≈35-fold) and the doxorubicin-resistant sub-line MCF-7/adr (≈10-fold), suggesting that the more lipophilic nature of the anthraquinones allows them to be taken up in the cells more readily than the more hydrophilic anthracycline. Significantly, after 96 h exposure, the MCF-7/adr cell line that expresses the MDR-1 phenotype was 1.6- and 4.6-fold more sensitive to alchemix and ICT2901 respectively compared with wild-type MCF-7 cells. In contrast to ICT2902 and ICT2903, alchemix and ICT2901 formed stable complexes with DNA (Table 1), however they were shown to be less potent topo IIα inhibitors. The MCF-7/adr cell line has been shown to possess a reduction in topo IIα protein compared to the MCF-7 cell line [26], which support why loss of activity of the two most potent topo IIα inhibitors ICT2902 and ICT2903 is observed.

The tumor suppressor p53 plays a central role in integrating various stress signals, in particular genotoxic stresses such as DNA damage, hypoxia, and oncogene activation [10, 27, 28]. It is mutated in more than 50% of human cancers [28] and has been shown to cause resistance to chemotherapy [29]. Accordingly, the development of drugs that act independently of p53 or even exploit defective p53 as a means of preferential toxicity is very important [29, 30]. The anthraquinones investigated herein are relatively unaffected by the p53 status of colorectal HCT116 cells, as only 1.5–3-fold loss of cytotoxicity was observed in the p53-null cells after 96 h. In addition, the MCF-7/adr cell line, that harbors a mutation in p53 [31], demonstrated slightly increased sensitivity to alchemix and ICT2901. Overall results from the four cell lines investigated indicate that p53 plays a negligible part in mediating the cytotoxicity of these two agents.

DNA damage is known to elicit a multifaceted cellular response that includes activation of DNA repair pathways, cell cycle checkpoints, and programmed cell death [30]. The latter may occur by several molecular mechanisms [32]. Apoptosis is one of the mechanisms by which chemotherapeutic agents might induce cancer cell demise [33]. There is increasing evidence that an inability to engage apoptosis can represent a resistance mechanism to cytotoxic drugs [34]. In regard to alchemix and the three analogues, it was desirable to investigate whether their cytotoxic potency was linked with apoptosis and/or necrosis. Data obtained from our studies appeared to show an SAR between increase in sidechain length of the three novel compounds (ICT2901–3), potency in DNA alkylation and increase in number of apoptotic and necrotic cells after short term (1 h) drug exposure. Interestingly, alchemix was found to be outside this SAR, implying differences in its mechanism of action. Early analysis (3 h) of cell cycle phase perturbations may also suggest a difference in mechanism of action as a higher number of G1 cells appeared to be arrested by alchemix treatment. This ability to perturb cells in G1 phase cells in the early stages after drug treatment may add significantly to the overall efficacy of alchemix.

DNA double strand breaks (DSBs) or damage at replication forks can be detected by phosphorylation of histone 2AX variant to form γH2AX focus formation. The role of γH2AX is to recruit DNA repair and cell cycle checkpoint proteins required for the efficient processing of DNA lesions [35]. All four compounds investigated in this study caused γH2AX phosphorylation after longer recovery times (24 h and 48 h). Intriguingly, significant γH2AX phosphorylation after short-term exposure (3 h) was only observed for ICT2901. As DNA interstrand crosslinking with naked DNA did not occur (supporting information, Figure S1), it is possible that the ICT2901-induced DNA damage and subsequent γH2AX phosphorylation arise after processing or signaling DNA damage.

In support for the adduct formation we observed that alchemix, ICT2901 and ICT2903 are all potentiated in the absence of the excision repair gene ERCC1, which is involved in NER, homologous recombination and inter-strand crosslink repair [36]. The UV5 cell line is defective in the XPD protein, which is involved in NER and crosslink repair [37], but not homologous recombination [38]. Since only the UV4 and not the UV5 cell line was sensitive to ICT2901 and ICT2903, it implicates that homologous recombination is involved in the response to these agents. Indeed, the irs1SF and NM3 cell lines defective in the recombination proteins XRCC3 and XRCC9 (FANCG) were both highly resistant to ICT2901 and ICT2903. This is in sharp contrast to the sensitivity of these cells to crosslinking agents and topo II inhibitors [39, 40]. These data demonstrate a separation of function between commonly used anti-cancer treatments and ICT2901 and ICT2903. Furthermore, it demonstrates that the proteins involved early in homologous recombination (XRCC3, FANCG) are required to mediate the toxicity, while proteins involved late in homologous recombination (ERCC1) are required for survival. These data point to that a recombination intermediate is mediating the toxicity, especially of ICT2901 and ICT2903, but likely also alchemix. Furthermore, alchemix has a different toxicity pattern to the DNA repair defective cell lines as compared to ICT2901 and ICT2903, demonstrating that it has a distinct mode of action. Since UV5 cells are sensitive to alchemix, we speculate that alchemix forms, in addition to a lesion similar to ICT2901 and ICT2903, also a DNA adduct repaired by NER. Mechanistically, we speculate that repair is initiated at the DNA adduct site to create a toxic lesion and that the intercalating part of the molecule interfere with proteins involved in the completion of recombination repair.

In summary, we have shown that subtle synthetic modifications to alchemix lead to significant changes in stability of DNA adducts and cellular pharmacology. The standard treatment for many solid and hematological cancers, despite limitations with regard to MDR,

is still based on cytotoxics such as the anthraquinone-based drugs doxorubicin or mitoxantrone. Despite the identification of cancer-specific molecular targets and the significant advances in a new generation of less toxic therapeutics the urgent need to treat relapsed patients with drug-resistant tumours remains. In this context, agents such as alchemix or ICT2901, that evade multiple resistance mechanisms, may provide an attractive solution to this unmet clinical need.

Acknowledgements

This work was supported by Yorkshire Cancer Research (Program Grant), White Rose Health Innovation Partnership (Project 010UoB) and Cancer Research UK (Program Grant C2259/A9994 to JAH). We also thank Dr Jason Gill for valuable discussions.

Appendix A. Supplementary data

Supplementary data including synthetic methods and **s**pectroscopic data of all compounds, DNA crosslinking (Figure S1) and CT DNA stabilization results (ΔT/t, Figure S2) can be found online at http://www.sciencedirect.com.

Conflicts of Interests

None.

REFERENCES

[1] Lown JW. Anthracycline and anthraquinone anticancer agents: current status and recent developments. Pharmacol Ther 1993;60:185-214.

[2] Murdock KC, Child RG, Fabio PF, Angier RB, Wallace RE, Durr FE, et al. Antitumor agents. 1. 1,4-Bis[(aminoalkyl)amino]-9,10-anthracenediones. J Med Chem 1979;22:1024-30.

[3] Johnson RK, Zee-Cheng RK, Lee WW, Acton EM, Henry DW, Cheng CC. Experimental antitumor activity of aminoanthraquinones. Cancer Treat Rep 1979;63:425-39.

[4] Zee-Cheng RK, Mathew AE, Xu PL, Northcutt RV, Cheng CC. Structural modification study of mitoxantrone (DHAQ). Chloro-substituted mono- and bis[(aminoalkyl)amino]anthraquinones. J Med Chem 1987;30:1682-6.
[5] Krapcho AP, Landi JJ, Jr., Shaw KJ, Phinney DG, Hacker MP, McCormack JJ. Synthesis and antitumor activities of unsymmetrically substituted 1,4-bis[(aminoalkyl)amino]anthracene-9,10-diones and related systems. J Med Chem 1986;29:1370-3.
[6] Krapcho AP, Getahun Z, Avery KL, Jr., Vargas KJ, Hacker MP, Spinelli S, et al. Synthesis and antitumor evaluations of symmetrically and unsymmetrically substituted 1,4-bis[(aminoalkyl)amino]anthracene-9,10-diones and 1,4-bis[(aminoalkyl)amino]-5,8-dihydroxyanthracene-9,10-diones. J Med Chem 1991;34:2373-80.
[7] Stefanska B, Dzieduszycka M, Martelli S, Borowski E. Synthesis of unsymmetrically substituted 1,4-bis[(aminoalkyl)amino]anthracene-9,10-diones as potential antileukemic agents. J Med Chem 1989;32:1724-8.
[8] Leslie EM, Deeley RG, Cole SP. Multidrug resistance proteins: role of P-glycoprotein, MRP1, MRP2, and BCRP (ABCG2) in tissue defense. Toxicol Appl Pharmacol 2005;204:216-37.
[9] Ueda K, Yoshida A, Amachi T. Recent progress in P-glycoprotein research. Anticancer Drug Des 1999;14:115-21.
[10] Leonard GD, Fojo T, Bates SE. The role of ABC transporters in clinical practice. Oncologist 2003;8:411-24.
[11] Li TK, Liu LF. Tumor cell death induced by topoisomerase-targeting drugs. Annu Rev Pharmacol Toxicol 2001;41:53-77.
[12] Chikamori K, Grabowski DR, Kinter M, Willard BB, Yadav S, Aebersold RH, et al. Phosphorylation of serine 1106 in the catalytic domain of topoisomerase II alpha regulates enzymatic activity and drug sensitivity. J Biol Chem 2003;278:12696-702.
[13] Pors K, Paniwnyk Z, Ruparelia KC, Teesdale-Spittle PH, Hartley JA, Kelland LR, et al. Synthesis and biological evaluation of novel chloroethylaminoanthraquinones with potent cytotoxic activity against cisplatin-resistant tumor cells. J Med Chem 2004;47:1856-9.
[14] Pors K, Shnyder SD, Teesdale-Spittle PH, Hartley JA, Zloh M, Searcey M, et al. Synthesis of DNA-directed pyrrolidinyl and piperidinyl confined alkylating chloroalkylaminoanthraquinones: potential for development of tumor-selective N-oxides. J Med Chem 2006;49:7013-23.
[15] Pors K, Paniwnyk Z, Teesdale-Spittle P, Plumb JA, Willmore E, Austin CA, et al. Alchemix: a novel alkylating anthraquinone with potent activity against anthracycline- and cisplatin-resistant ovarian cancer. Mol Cancer Ther 2003;2:607-10.
[16] Ponti M, Forrow SM, Souhami RL, D'Incalci M, Hartley JA. Measurement of the sequence specificity of covalent DNA modification by antineoplastic agents using Taq DNA polymerase. Nucleic Acids Res 1991;19:2929-33.
[17] Fox KR. Methods in molecular biology. 90, Drug-DNA interaction protocols. Totowa, N.J.: Humana Press, 1997.
[18] Wheelhouse RT, Jennings SA, Phillips VA, Pletsas D, Murphy PM, Garbett NC, et al. Design, synthesis, and evaluation of novel biarylpyrimidines: a new class of ligand for unusual nucleic acid structures. J Med Chem 2006;49:5187-98.
[19] Mosmann T. Rapid colorimetric assay for cellular growth and survival: application to proliferation and cytotoxicity assays. J Immunol Methods 1983;65:55-63.
[20] Johansson F, Allkvist A, Erixon K, Malmvarn A, Nilsson R, Bergman A, et al. Screening for genotoxicity using the DRAG assay: investigation of halogenated environmental contaminants. Mutat Res 2004;563:35-47.

[21] Mattes WB, Hartley JA, Kohn KW. DNA sequence selectivity of guanine-N7 alkylation by nitrogen mustards. Nucleic Acids Res 1986;14:2971-87.
[22] Smith PJ, Blunt NJ, Desnoyers R, Giles Y, Patterson LH. DNA topoisomerase II-dependent cytotoxicity of alkylaminoanthraquinones and their N-oxides. Cancer Chemother Pharmacol 1997;39:455-61.
[23] Bakker M, Renes J, Groenhuijzen A, Visser P, Timmer-Bosscha H, Muller M, et al. Mechanisms for high methoxymorpholino doxorubicin cytotoxicity in doxorubicin-resistant tumor cell lines. Int J Cancer 1997;73:362-6.
[24] Cummings J, Macpherson JS, Meikle I, Smyth JF. Development of anthracenyl-amino acid conjugates as topoisomerase I and II inhibitors that circumvent drug resistance. Biochem Pharmacol 1996;52:979-90.
[25] Masta A, Gray PJ, Phillips DR. Molecular basis of nitrogen mustard effects on transcription processes: role of depurination. Nucleic Acids Res 1994;22:3880-6.
[26] Lage H, Aki-Sener E, Yalcin I. High antineoplastic activity of new heterocyclic compounds in cancer cells with resistance against classical DNA topoisomerase II-targeting drugs. Int J Cancer 2006;119:213-20.
[27] Levine AJ. p53, the cellular gatekeeper for growth and division. Cell 1997;88:323-31.
[28] Vogelstein B, Lane D, Levine AJ. Surfing the p53 network. Nature 2000;408:307-10.
[29] O'Connor PM, Jackman J, Bae I, Myers TG, Fan S, Mutoh M, et al. Characterization of the p53 tumor suppressor pathway in cell lines of the National Cancer Institute anticancer drug screen and correlations with the growth-inhibitory potency of 123 anticancer agents. Cancer Res 1997;57:4285-300.
[30] Cheok CF, Verma CS, Baselga J, Lane DP. Translating p53 into the clinic. Nat Rev Clin Oncol 2011;8:25-37.
[31] Ogretmen B, Safa AR. Expression of the mutated p53 tumor suppressor protein and its molecular and biochemical characterization in multidrug resistant MCF-7/Adr human breast cancer cells. Oncogene 1997;14:499-506.
[32] Bai S, Goodrich DW. Different DNA lesions trigger distinct cell death responses in HCT116 colon carcinoma cells. Mol Cancer Ther 2004;3:613-9.
[33] Guerriero JL, Ditsworth D, Fan Y, Zhao F, Crawford HC, Zong WX. Chemotherapy induces tumor clearance independent of apoptosis. Cancer Res 2008;68:9595-600.
[34] Hickman JA, Boyle CC. Apoptosis and cytotoxins. Br Med Bull 1997;53:632-43.
[35] Bonner WM, Redon CE, Dickey JS, Nakamura AJ, Sedelnikova OA, Solier S, et al. GammaH2AX and cancer. Nat Rev Cancer 2008;8:957-67.
[36] Al-Minawi AZ, Lee YF, Hakansson D, Johansson F, Lundin C, Saleh-Gohari N, et al. The ERCC1/XPF endonuclease is required for completion of homologous recombination at DNA replication forks stalled by inter-strand cross-links. Nucleic Acids Res 2009;37:6400-13.
[37] De Silva IU, McHugh PJ, Clingen PH, Hartley JA. Defects in interstrand cross-link uncoupling do not account for the extreme sensitivity of ERCC1 and XPF cells to cisplatin. Nucleic Acids Res 2002;30:3848-56.
[38] Savolainen L, Cassel T, Helleday T. The XPD subunit of TFIIH is required for transcription-associated but not DNA double-strand break-induced recombination in mammalian cells. Mutagenesis 25:623-9.
[39] Caldecott K, Jeggo P. Cross-sensitivity of gamma-ray-sensitive hamster mutants to cross-linking agents. Mutat Res 1991;255:111-21.
[40] Lundin C, Schultz N, Arnaudeau C, Mohindra A, Hansen LT, Helleday T. RAD51 is involved in repair of damage associated with DNA replication in mammalian cells. J Mol Biol 2003;328:521-35.

Table Legends

Table 1 Thermal denaturation of CT-DNA in the presence of the four alkylating agents

Below the Table: [a] Anthraquinones were subjected to DNA thermal melting (denaturation) studies using CT-DNA at a fixed 5:1 (50 μM DNA:10 μM compound) ratio. The DNA-anthraquinone mixtures were incubated at 37 °C and evaluated at 0, 4, 8 and 24 h. Results for each compound are from three separate determinations with mean T_m values ± 0.1 ºC. See materials and methods for details.

Table 2 Growth Inhibition of Alkylating Anthraquinones against Wild-Type and p53 Null HCT116 Carcinoma Cell Lines

Below the Table: All IC_{50} values are in nM and the data represent the means of three independent experiments ± SD. RF = resistance factor (IC_{50} in resistant cell line/IC_{50} in parent cell line).

Table 3 Growth Inhibition of Alkylating Anthraquinones against MCF-7 and MCF-7/adr Carcinoma Cell Lines

Below the Table: All IC_{50} values are in nM except where indicated for doxorubicin. The data represent the means of three independent experiments ± SD. RF = resistance factor (IC_{50} in resistant cell line/IC_{50} in parent cell line).

Table 4 Growth Inhibition of Alkylating Anthraquinones against A Panel of CHO Cell Lines with Gene Defects

Below the Table: The data represent the means of two independent experiments ± SD after treatments with indicated compounds. SR = sensitivity factor (IC_{50} in parent cell line/IC_{50} in defective cell line).

Figure Legends

Fig. 1 Alkylating anthraquinones

Fig. 2 Effects of alchemix, ICT2901, ICT2902, and ICT2903 on *Taq* DNA polymerase elongation of plasmid pBR322. Control: unmodified DNA; The solid triangles represent increasing of compounds; from left to right, these are: 1, 2.5, 10 μM for HN2 (mechlorethamine) and 1, 5, 25, 100 nM for anthraquinones.

Fig. 3 Effects of the indicated compounds on decatenation of kinetoplast DNA in the presence of topo IIα. Each compound was tested at 1 μM (A) and 0.1 μM (B).

Fig. 4 Anthraquinone-induced changes in the cell cycle phase distribution. Parental $HCT116^{p53+/+}$ cells were treated with the indicated drug at IC_{80} (alchemix = 188 nM, ICT2901 = 100 nM, ICT2902 = 177 nM and ICT2903 = 339 nM) for 1 h followed by a 3, 24, 48 h incubation in anthraquinone-free medium. The cell cycle distribution was determined by propidium iodide staining and flow cytometry. The data are normalized to control untreated

cells and presented as fold change (represented by the broken line) from three independent experiments.

Fig. 5 Anthraquinone-induced apoptotic cell death. Parental HCT116$^{p53+/+}$ cells were treated with the indicated compound at IC_{80} (alchemix = 188 nM, ICT2901 = 100 nM, ICT2902 = 177 nM and ICT2903 = 339 nM) for 1 h followed by 24 h incubation in anthraquinone-free medium. Cells were collected and analysed using the TUNEL assay. The treated cells (grey bars) and control cells (white bars) represent the means of three independent experiments ± SD.

Fig. 6 Anthraquinone-induced necrotic cell death. Parental HCT116$^{p53+/+}$ cells were treated with the indicated compound at IC_{80} (alchemix = 188 nM, ICT2901 = 100 nM, ICT2902 = 177 nM and ICT2903 = 339 nM) for 1 h followed by 24 or 48 h incubation in anthraquinone-free medium. Cells were collected and analysed using the Trypan Blue assay. The treated cells (grey bars) and control cells (white bars) represent the means of three independent experiments ± SD.

Fig. 7 Anthraquinone-induced changes in γH2AX foci. Parental HCT116$^{p53+/+}$ cells were treated with the indicated compound at IC_{80} (alchemix = 188 nM, ICT2901 = 100 nM, ICT2902 = 177 nM and ICT2903 = 339 nM) for 1 h followed by a 3, 24, 48 h incubation in anthraquinone-free medium. Cells were then stained with Phospho-Histone H2AX (Ser139) antibody as described in materials and methods. The treated cells (black bars) and control cells (grey bars) represent the means of three independent experiments ± SD.

Table 1

	Induced ΔT_m (°C)[a]			
Compound	**0 h**	**4 h**	**8 h**	**24 h**
Alchemix	11.0	11.0	10.9	9.5
ICT2901	14.8	14.9	14.8	13.6
ICT2902	7.0	4.8	4.7	1.3
ICT2903	6.5	3.6	3.2	-0.8

Table 2

	1 hour			96 hours		
Compound	**p53+/+**	**p53-/-**	**RF**	**p53+/+**	**p53-/-**	**RF**
Alchemix	48 ± 13	53.5 ± 20	1.1	28.5 ± 5.6	45 ± 11	1.6
ICT2901	14 ± 4.7	23 ± 13	1.7	13.3 ± 3.3	43 ± 13	3.3
ICT2902	34 ± 16	52 ± 39	1.6	26 ± 10.	55 ± 16.5	2.1
ICT2903	76 ± 17	98 ± 29	1.3	66.8 ± 7.2	91 ± 44	1.4

Table 3

	1 hour			96 hours		
Compound	**MCF-7**	**MCF-7/adr**	**RF**	**MCF-7**	**MCF-7/adr**	**RF**
Alchemix	85 ± 36	73 ± 16.	0.85	48 ± 10	28.6 ± 8.8	0.6
ICT2901	15.5 ± 6.9	5.3 ± 0.9	0.34	13.5 ± 6.4	2.9 ± 0.8	0.2
ICT2902	26 ± 14	37.25 ± 0.78	1.5	36.3 ± 4.1	52.5 ± 17.7	1.4
ICT2903	91 ± 24	314 ± 1295	3.5	92 ± 28	320 ± 99	3.5
Doxorubicin	6.1 ± 1.7 µM	> 100 µM	> 17	218 ± 91	> 10 µM	> 45

Table 4

Cell line	Gene defect	Alchemix		ICT2901		ICT2903	
		IC_{50} [nM]	SR	IC_{50} [nM]	SR	IC_{50} [µM]	SR
AA8		42.9 ± 6.8		11.5 ± 5.0		0.2 ± 0.0	
UV4	ERCC1	13.3 ± 1.4	3.2	6.0 ± 4.5	1.9	0.1 ± 0.0	1.3
UV5	ERCC2	20.8 ± 1.2	2.1	15.4 ± 12.6	0.7	0.2 ± 0.0	0.8
EM9	XRCC1	36.4 ± 12.5	1.2	12.8 ± 10.1	0.9	0.4 ± 0.2	0.5
irs1SF	XRCC3	100.9 ± 46.4	0.4	35.9 ± 32.9	0.3	7.0 ± 1.6	0.0
NM3	XRCC9	65.4± 72.6	0.7	144.8 ± 141.9	0.1	8.6 ± 1.1	0.0
V3-3	XRCC7	92.9 ± 21.6	0.5	34.2 ± 29.2	0.3	0.6 ± 0.0	0.3

Figure 1

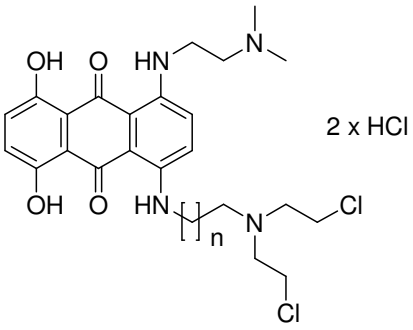

Alchemix: n = 1
ICT2901: n = 2
ICT2902: n = 3
ICT2903: n = 4

Figure 2

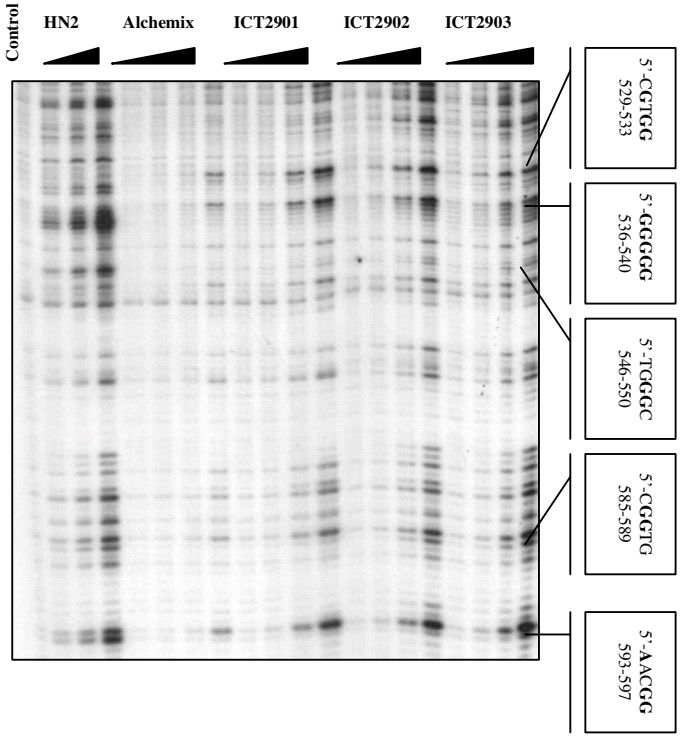

Figure 3

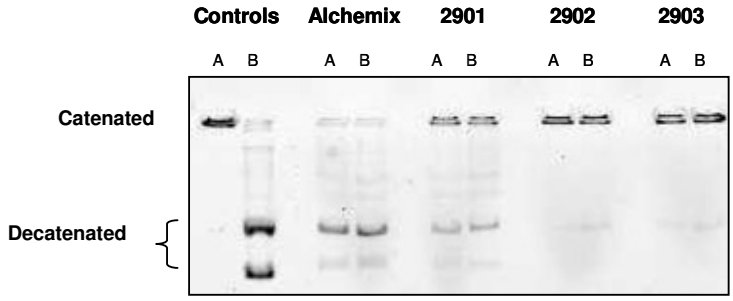

Figure 4

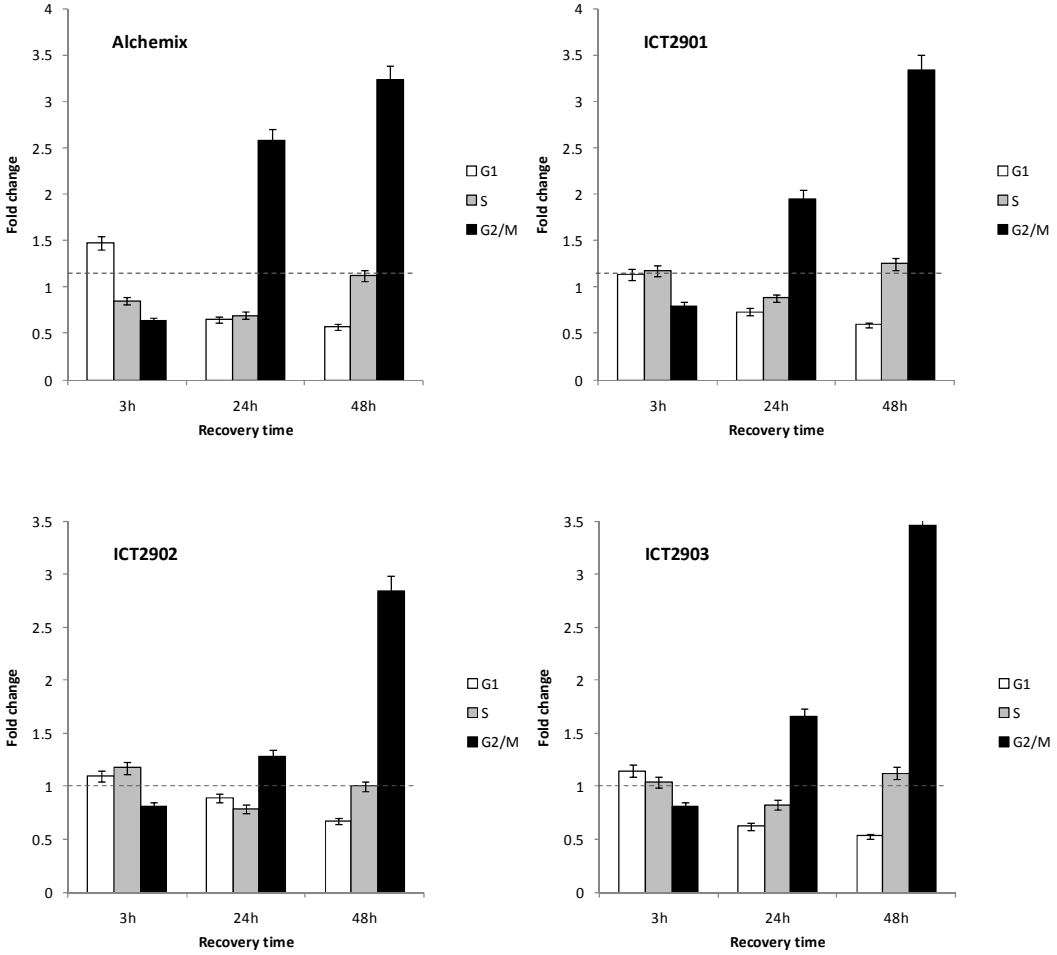

Figure 5

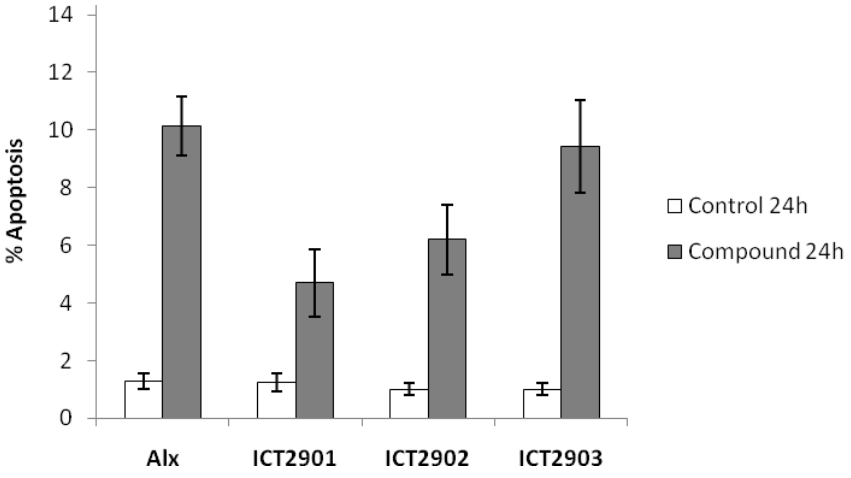

Figure 6

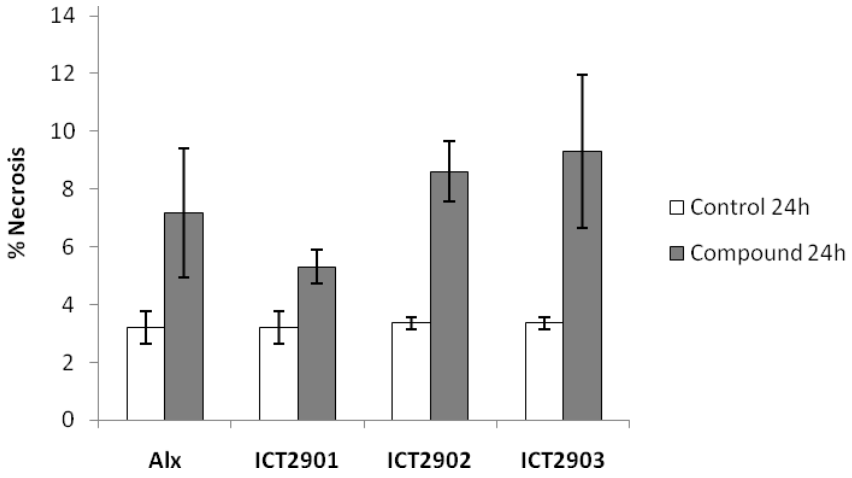

Figure 7

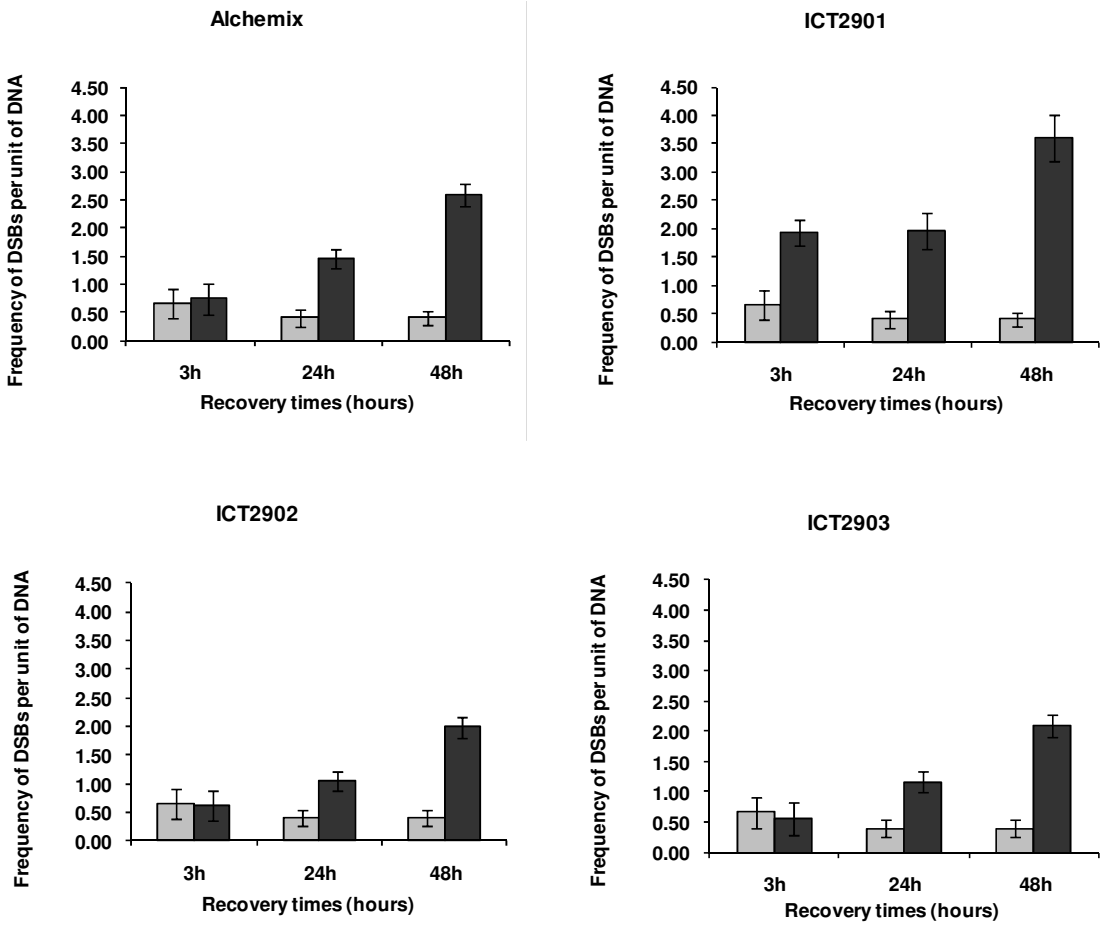

Table of Contents Graphic

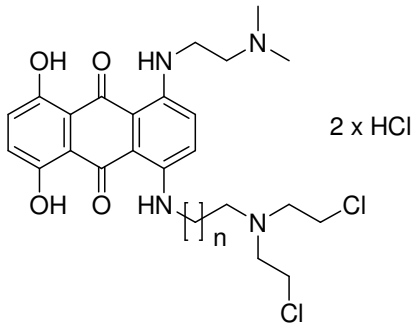

Alchemix: n = 1
ICT2901: n = 2
ICT2902: n = 3
ICT2903: n = 4